Electronic Supplementary Information: Inhibition-mediated changes in prolyl oligopeptidase dynamics possibly related to α-synuclein aggregation

Katarzyna Walczewska-Szewc*[a], Jakub Rydzewski [a], and Aneta Lewkowicz [b]

[a.] Institute of Physics, Faculty of Physics, Astronomy and Informatics, Nicolaus Copernicus University, Grudziądzka 5, 87-100 Toruń, Poland
[b.] Faculty of Mathematics, Physics and Informatics, Gdansk University, Wita Stwosza 57, 80-952 Gdańsk, Poland
* kszewc@fizyka.umk.pl

Inhibitors

In this work we analysed three different PREP inhibitors:

KYP 2047 (IUPAC name: 1-[1-(4-phenylbutanoyl)pyrrolidine-2-carbonyl]pyrrolidine-2-carbonitrile) – covalent bound to PREP[1, 2]

SUAM 1221 (IUPAC name: 4-phenyl-1-[(2S)-2-(pyrrolidine-1-carbonyl)pyrrolidin-1-yl]butan-1-one)

S 17092(IUPAC name: [(2S,3aS,7aS)-2-(1,3-thiazolidine-3-carbonyl)-2,3,3a,4,5,6,7,7a-octahydroindol-1-yl]-[(1R,2R)-2-phenylcyclopropyl]methanone)

Molecular docking

Three known PREP inhibitors were used in this study. Potential binding sites for all ligands were determined using the Schrodinger/Glide docking package. For each ligand, we performed three dockings. The first, so-called blind docking, was performed without choosing the approximate binding site - the drug could dock anywhere within the protein. The second docking restricted the potential poses to the vicinity of the active centre of PREP. These two docking experiments were performed using PREP in open form (obtained after MD equilibration). The last docking, also restricting poses to the enzyme's active centre, uses PREP in the closed-form (PDB ID: 3DDU). All modelling was performed using flexible docking.

The poses with the lowest docking energy from the third modelling were chosen as the starting point for the MD simulations. Table S1 lists the docking energies for the individual poses. In blind docking, for open PREP, the drug is more likely docked inside the β-propeller channel. For closed PREP, the most energetically favourable poses were around the active centre. The best pose obtained for KYP 2047 agrees with the known crystal structure of KYP 2047 bound to porcine PREP [1] (PDB ID:4AN0, 98% sequence similarity with human PREP). The calculated binding affinities of all inhibitors to PREP were comparable.

Table S1 Docking values obtained from three docking experiments; binding energies from MM-PBSA modelling.

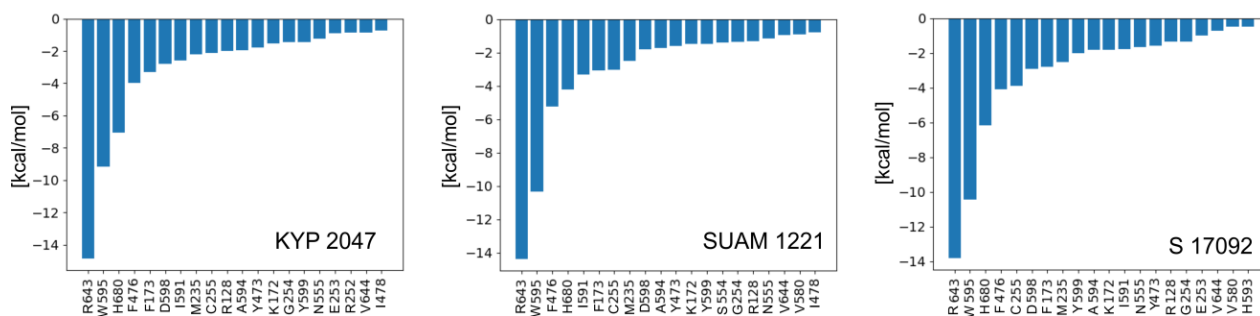| Ligand	Blind docking (open PREP)	Active site docking (open PREP)	Active site docking (closed PREP)
KYP2047	-6.02	-4.47	-8.09
SUAM1221	-4.73	-4.67	-8.37
S17092	-5.23	-4.53	-7.54

Figure S1: Residues with the highest contribution to the energy of binding of ligands at the active site of PREP.

The contribution of individual residues during docking of three ligands is shown in Figure S1. These computed interactions were found to be similar in all cases. Of particular interest were four residues R643, W595, H680 and F476, located in the active centre of PREP, which gave the highest contribution to the energy of binding.

Ligands force-field parameters validation

The first attempt to experimentally verify the correctness of the ligand parameters was to compare the structure obtained after minimisation of the system for the given parameters with the structure obtained from the X-ray diffraction experiment. Due to the limited availability of experimental data, such comparison was possible only for KYP 2047, which perfectly agrees with the experimental structure.

To further validate the parameters of the drugs, we calculated the octanol-water partitioning coefficients (log P), which were compared with available experimental data. The mean log P for the optimal brain penetration is 2.1[3]. The octanol-water partitioning free energies were determined using the Bennett Acceptance Ratio (BAR) approach implemented in MDPOW- a python package that automates the calculation of solvation free energies via molecular dynamics (MD) simulations and facilitates the computation of partition coefficients (https://github.com/Becksteinlab/mdpow).

First, optimised structures of KYP 2047, SUAM 1221, and S 17092 were solvated (in water or the water-octanol mix) in a periodic dodecahedron simulation cell with a minimal distance of 2 nm to the nearest box surface. Solvated systems were first energy minimized and relaxed with a short, five picoseconds NPT MD simulation. Then an initial NPT equilibrium simulation (T=300 K, P=1 bar) with time step 2 fs was carried out for 50 ns. After the equilibration phase, the 25 ns free energy calculations began, using the last frame of the equilibrium simulation as the starting point. The NPT ensemble MD simulations were performed at T=300 K, with all other parameters kept as MDPOW default (for CHARMM force-field simulation). Simulation parameters for water and octanol simulations were identical.

The obtained values of log P for three ligands slightly differs from those determined experimentally (for KYP 2047 and SUAM 1221). Nevertheless the trend of increasing log P from experiment and XlogP3 calculations is maintained.

Table S2: Experimental verification of parameters: IC50-values against porcine PREP with references; logP - water-octanol partition coefficient from experiment; partition coefficient calculated with XlogP3 server (XlogP3) and obtained via MD simulations using MDPOW (MD logP).

Ligand	IC_{50}	logP	XlogP3[4]	MD logP
KYP2047	0.2[5]	1.6[5]	2.33	2.18 (0.02)
SUAM1221	1.5[6]	1.8[5]	2.51	2.35 (0.03)
S17092	2.0[7]	-	3.5	3.028 (0.03)

Summary of MD runs

Table S3: Summary of MD simulations

System	lp	RMSD Cα [Å]	Simulation time [μs]	Inter-domain opening
APO	1	2.63 (1.17)	0.5	yes
	2	1.57 (0.27)	0.5	no
	3	1.57 (0.16)	0.5	no
	4	1.58 (0.2)	0.5	no
	5	3.43 (1.39)	0.5	yes
	6	1.58 (0.16)	1.0	no
	7	1.91 (0.41)	1.0	no
	8	5.58 (3.40)	1.0	yes
	9	1.79 (0.18)	1.0	no
	10	1.81 (0.48)	1.0	no
KYP2047	1	1.46 (0.12)	0.5	no
	2	1.43 (0.13)	0.5	no
	3	1.31 (0.10)	0.5	no
	4	1.35 (0.13)	0.5	no
	5	1.52 (0.19)	0.5	no
SUAM1221	1	1.45 (0.11)	0.5	no
	2	1.53 (0.18)	0.5	no
	3	1.44 (0.14)	0.5	no
	4	1.52 (0.15)	0.5	no
	5	1.38 (0.13)	0.5	no
S17092	1	1.70 (0.20)	0.5	no
	2	1.39 (0.14)	0.5	no
	3	1.49 (0.14)	0.5	no
	4	1.36 (0.14)	0.5	no
	5	1.62 (0.15)	0.5	no

Dynamics od PREP
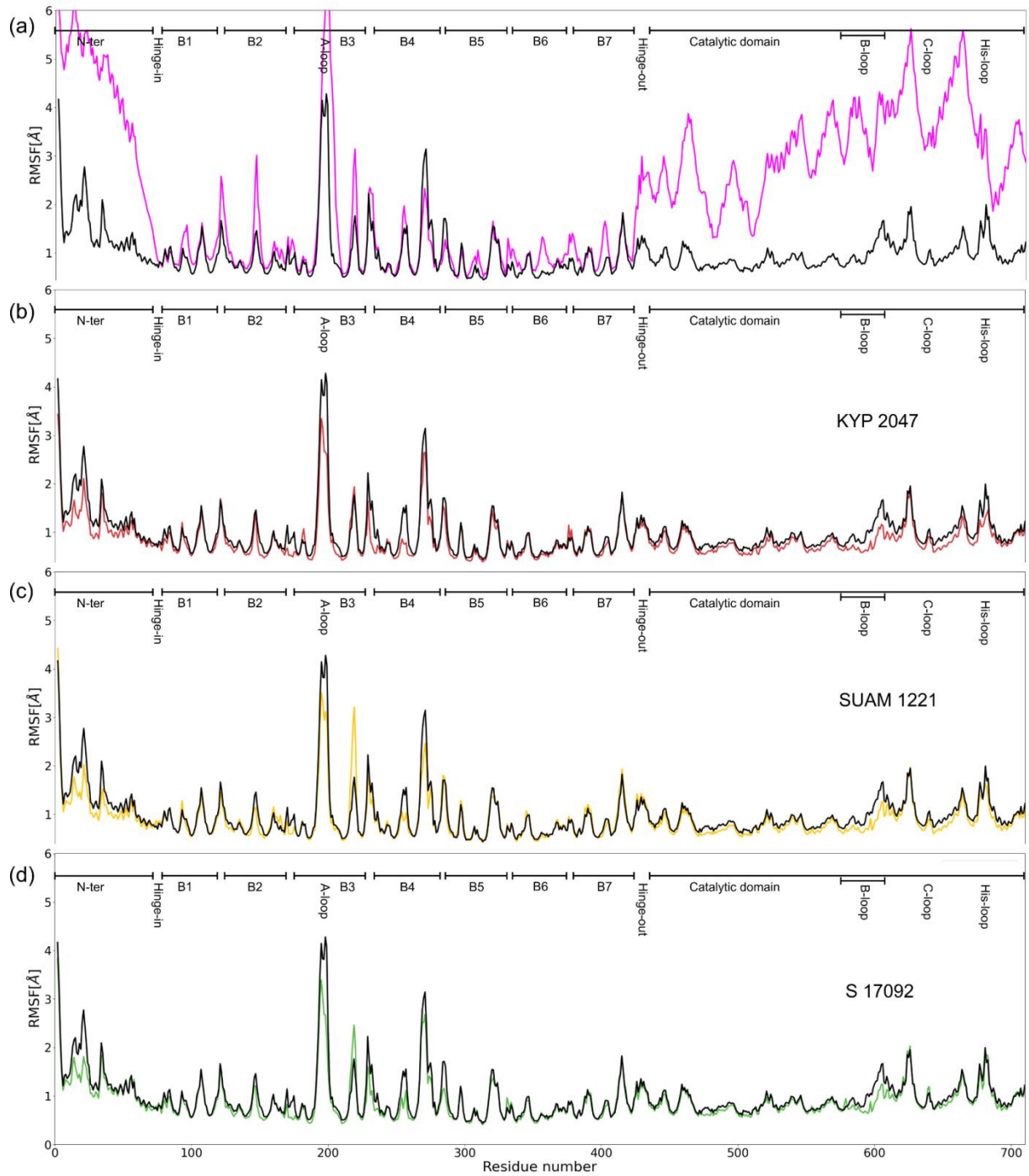
Figure S2: Comparison of the Root Mean Square Fluctuations of PREP in APO (top) and ligand-bound models. APO simulations with and without interdomain opening are shown in magenta and black curves, respectively.
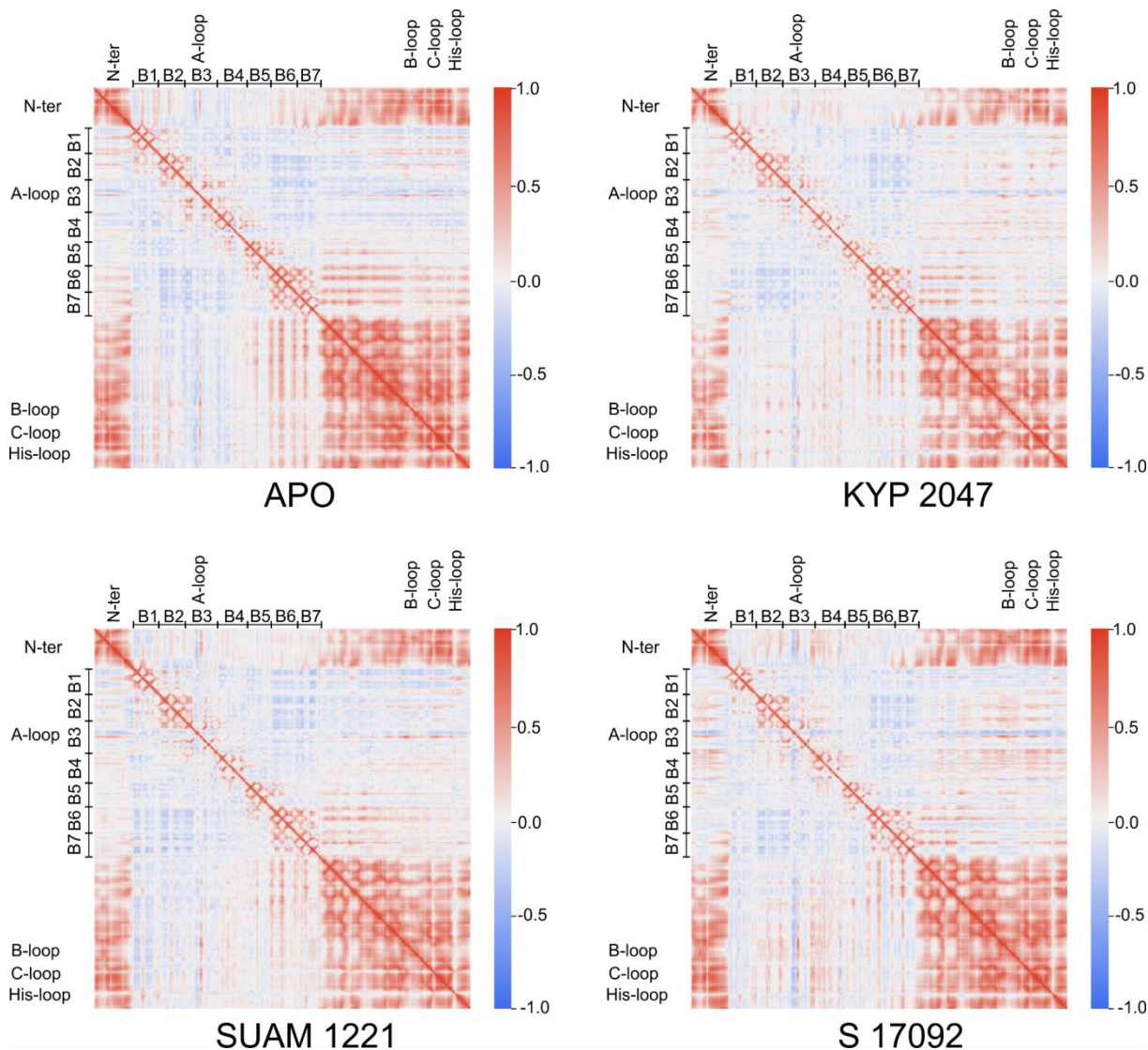
Figure S3: Correlation matrices calculated from 5x500 ns MD trajectories data for APO, KYP 2047, SUAM 1221, and S 17092 systems. Couplings among parts of PREP in each system were analysed using the dynamic cross-correlation matrices[8].
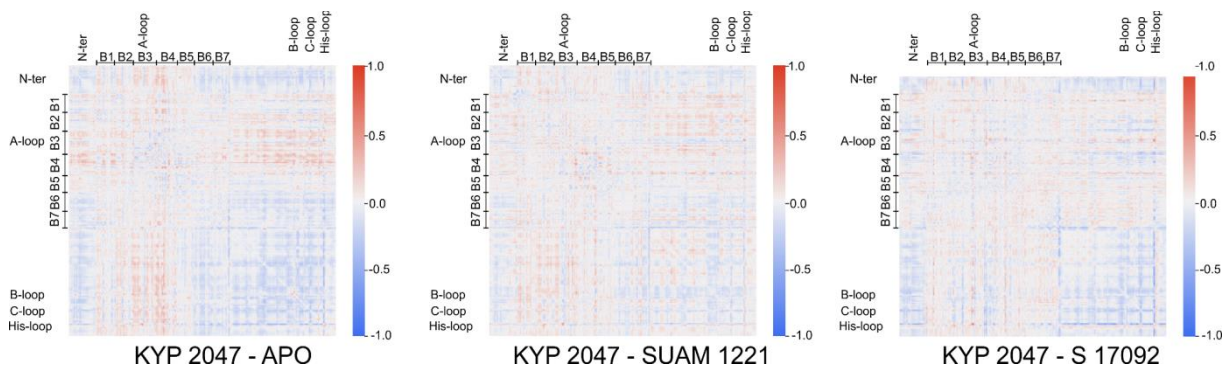

Figure S4: Differences in the dynamic cross-correlation matrices.
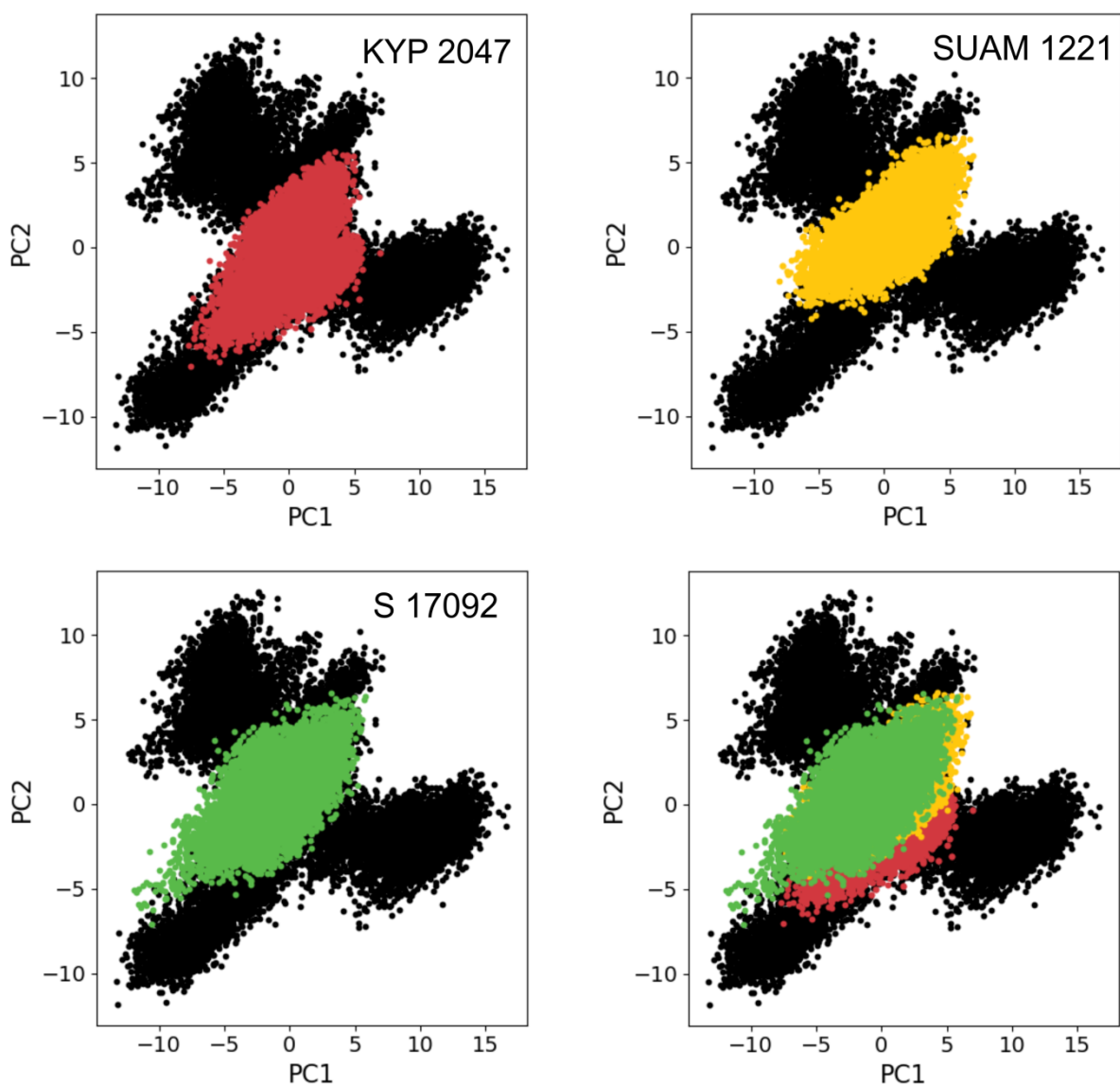
Figure S5: Principle Components Analysis of all systems. APO (black) compared with KYP2047 (red), SUAM 1221 (yellow), and S 17092 (green). The dimensionality reduction was performed using mdtraj and scikit-learn Python packages.

APO   KYP 2047   SUAM 1221   S 17092
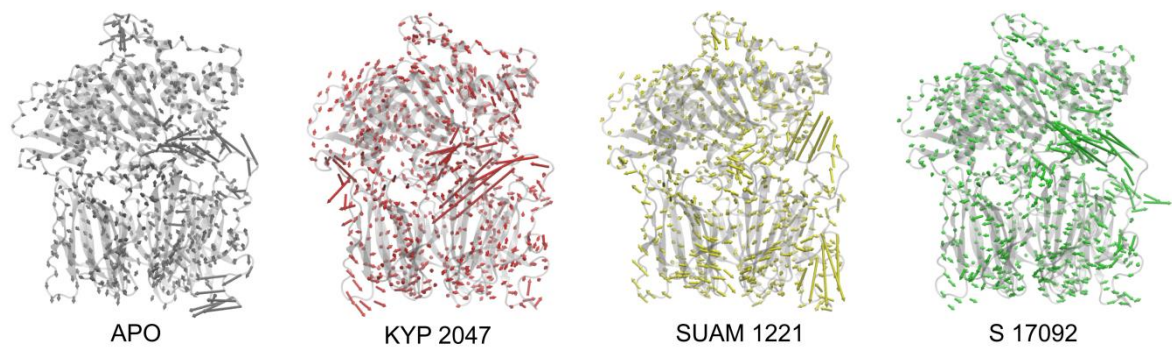
Figure S6: Normal modes analysis of all systems. The most prominent motion vectors are shown in colours. The normal modes was calculated using ProDy[9] package and visualised using Normal Modes Wizard at VMD.
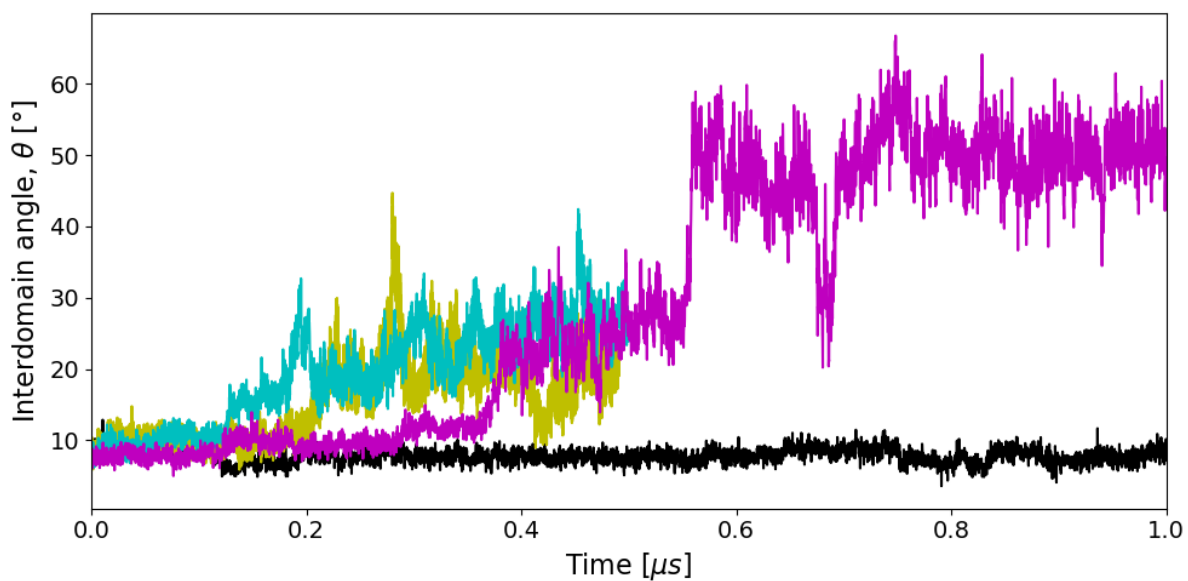
Figure S7: Time-series of the inter-domain angle change for four APO simulations. Three runs that capture the opening of the domains are shown in cyan, yellow, and magenta. The exemplary run of fully-closed run is shown in black.
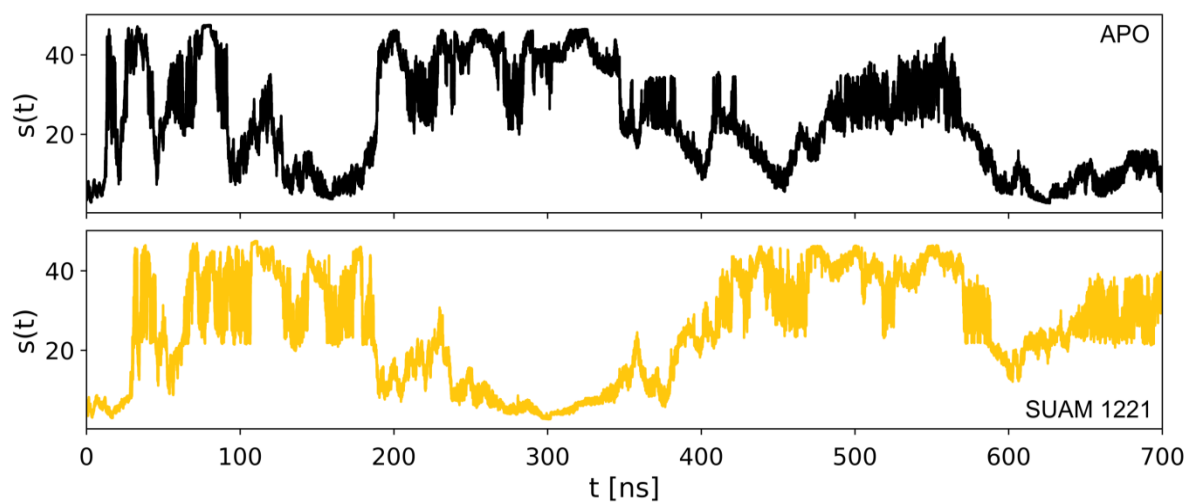

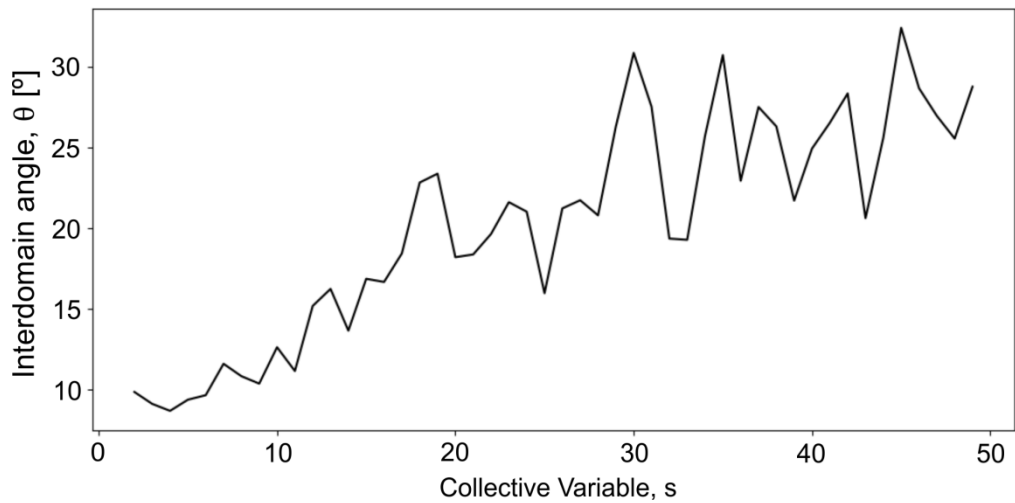Figure S8: Time-series of Collective Variable, s, for each system: APO (black) and SUAM 1221 (yellow).

Figure S9: The dependence between the collective variable, s, used in the metadynamics simulations and the interdomain angle.
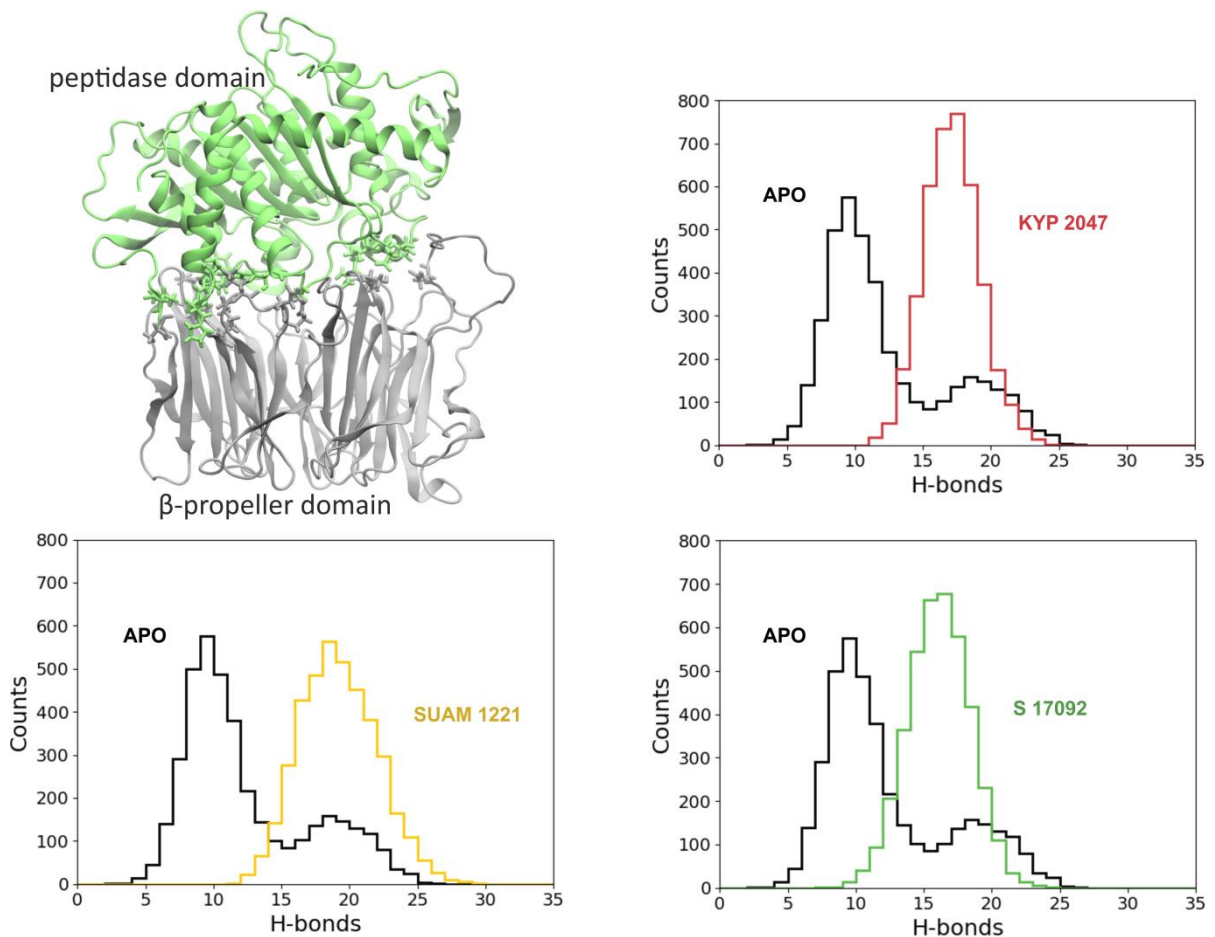

Figure S10: Number of H-bonds between the peptidase and β-propeller domains for each system.

Dynamics of ligands in the PREP cavity

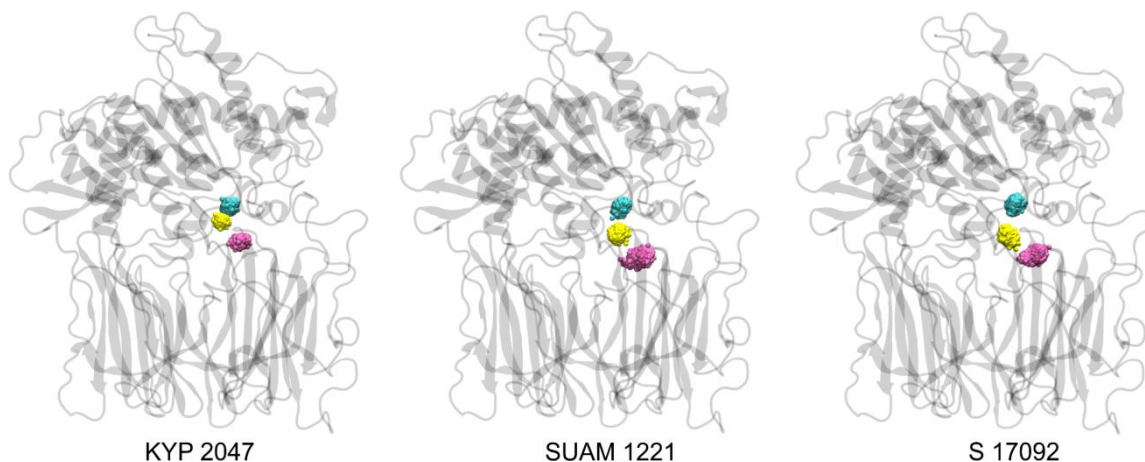KYP 2047   SUAM 1221   S 17092

Figure S11: Distribution of ligands position during simulation. Centres of mass of ligands P1, P2, and P3 groups are shown by cyan, yellow, and magenta dots, respectively. Covalent binding of KYP 2047 significantly reduced its mobility inside the cavity.
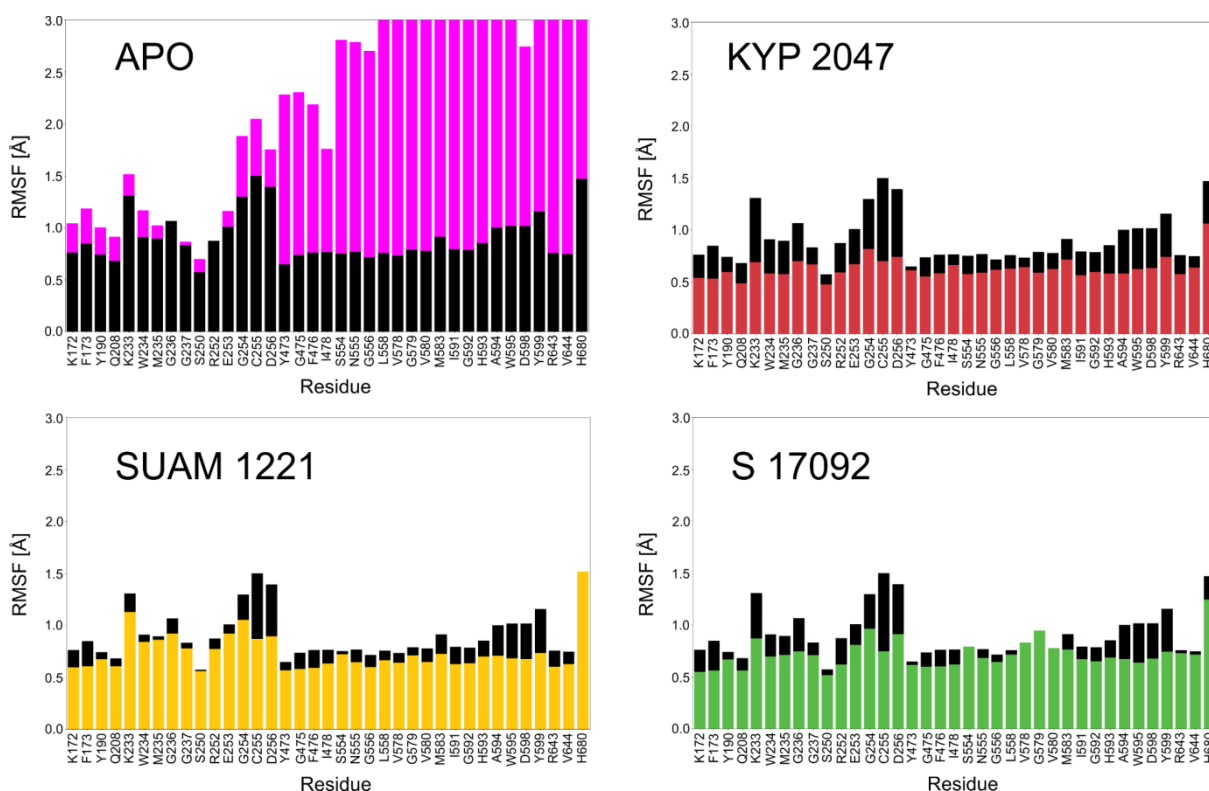

Figure S12: Root Mean Square Fluctuations of residues within 6Å from the ligand. Cα RMSD calculations indicate a trend for decreased flexibility of such residues and this is apparent for all PREP-inhibitor systems. Comparison with the APO results for both open (magenta) and closed (black) state indicates that existence of inhibitor, apart keeping the protein in a closed form, slightly decrease the overall flexibility of residues from the binding region. The most affected are residues in close contact with the ligand.

Solvent accessible surface analysis

We analysed the changes of the protein surface upon binding of different ligands taking into account the differences in solvent accessible area (SASA). SASA of each residue across each frame in a MD trajectory was computed using MDTraj Python library[10]. The code implements the Shrake and Rupley algorithm[11], with the Golden Section Spiral algorithm to generate the sphere points.

In Figure S8 a we show the average value of SASA for four residues which show the biggest change. Figure S8 b and c show the differences between KYP 2047 -- SUAM 1221 (b) and KYP 2047 -- S 17092 (c), blue colour denotes residues which are more solvent accessible in KYP, red colour shows residues which are more buried in KYP 2047 than in other cases.
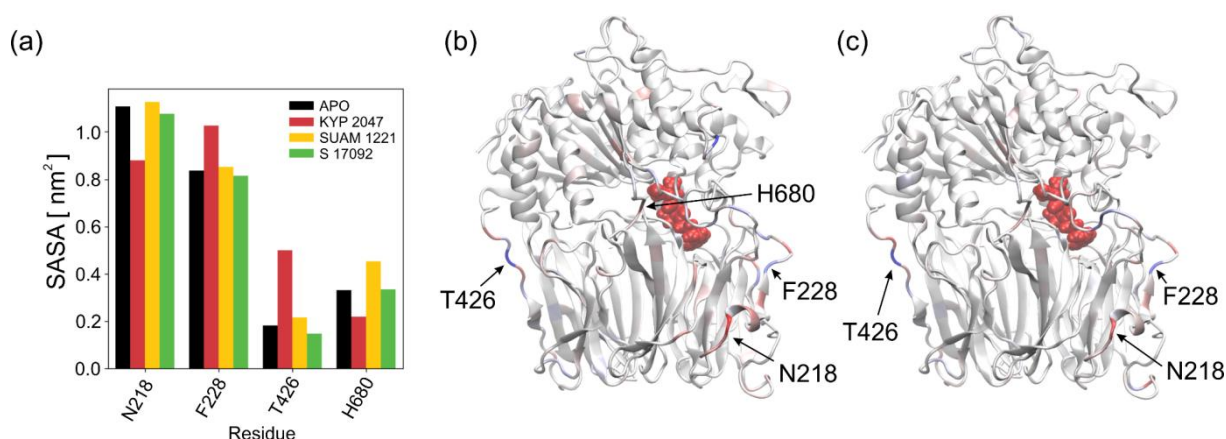

Figure S13: Solvent Accessible Surface analysis. Residues with the biggest differences in calculated SASA for different ligands.

References

1.   K. Kaszuba, T. Róg, R. Danne, P. Canning, V. Fülöp, T. Juhász, Z. Szeltner, J. F. St Pierre, A. García-Horsman, P. T. Männistö, M. Karttunen, J. Hokkanen and A. Bunker, *Biochimie*, 2012, **94**, 1398-1411.
2.   S. Guardiola, R. Prades, L. Mendieta, A. J. Brouwer, J. Streefkerk, L. Nevola, T. Tarragó, R. M. J. Liskamp and E. Giralt, *Cell Chemical Biology*, 2018, **25**, 1031-1037.e1034.
3.   H. Pajouhesh and G. R. Lenz, *NeuroRx : the journal of the American Society for Experimental NeuroTherapeutics*, 2005, **2**, 541-553.
4.   T. Cheng, Y. Zhao, X. Li, F. Lin, Y. Xu, X. Zhang, Y. Li, R. Wang and L. Lai, *Journal of chemical information and modeling*, 2007, **47**, 2140-2148.
5.   E. M. Jarho, J. I. Venäläinen, J. Huuskonen, J. A. Christiaans, J. A. Garcia-Horsman, M. M. Forsberg, T. Järvinen, J. Gynther, P. T. Männistö and E. A. Wallén, *Journal of medicinal chemistry*, 2004, **47**, 5605-5607.
6.   H. Barelli, A. Petit, E. Hirsch, S. Wilk, G. De Nanteuil, P. Morain and F. Checler, *Biochemical and biophysical research communications*, 1999, **257**, 657-661.
7.   E. A. Wallén, J. A. Christiaans, S. M. Saario, M. M. Forsberg, J. I. Venäläinen, H. M. Paso, P. T. Männistö and J. Gynther, *Bioorganic & medicinal chemistry*, 2002, **10**, 2199-2206.
8.   K. Kasahara, I. Fukuda and H. Nakamura, *PLOS ONE*, 2014, **9**, e112419.
9.   A. Bakan, L. M. Meireles and I. Bahar, *Bioinformatics*, 2011, **27**, 1575-1577.

10.   Robert T. McGibbon, Kyle A. Beauchamp, Matthew P. Harrigan, C. Klein, Jason M. Swails, Carlos X. Hernández, Christian R. Schwantes, L.-P. Wang, Thomas J. Lane and Vijay S. Pande, *Biophysical journal*, 2015, **109**, 1528-1532.
11.   A. Shrake and J. A. Rupley, *Journal of molecular biology*, 1973, **79**, 351-371.